Pancreatic Mass Segmentation Using TransUNet Network

Fael Faray de Paiva, Alexandre de Carvalho Araujo[a], João Dallyson Sousa de Almeida[b] and Anselmo C. de Paiva[c]
Núcleo de Computacão Aplicada — Universidade Federal do Maranhão (UFMA), São Luís, MA, Brazil

Keywords: Mass, Pancreas, TransUNet, Transformer.

Abstract: Currently, one of the major challenges in computer vision applied to medical imaging is the automatic segmentation of organs and tumors. Pancreatic cancer, in particular, is extremely lethal, primarily due to the major difficulty in early detection, resulting in the disease being identified only in advanced stages. Recently, new technologies, such as deep learning, have been used to identify these tumors. This work uses the TransUNet network for the task, as convolutional neural networks (CNNs) are extremely effective at capturing features but present limitations in tasks that require greater context. On the other hand, transformer blocks are designed for sequence-to-sequence tasks and have a high capacity for processing large contexts; however, they lack spatial precision due to the lack of detail. TransUNet uses the Transformer as an encoder to enhance the capacity to process content globally, while convolutional neural networks are employed to minimize the loss of features during the process. Among the experiments presented herein, one used image pre-processing techniques and achieved an average Dice score of 42.60±1.97%. The second experiment, a crop was applied to the mass region, reaching an average Dice score of 79.67±2.31%.

1 INTRODUCTION

The pancreas plays a fundamental role in controlling energy consumption and metabolism in the human body, with both exocrine and endocrine functions (Czako et al., 2009). The exocrine function is responsible for the production and secretion of essential digestive enzymes, such as lipases, proteases, and amylases, which are indispensable for the digestive process. These enzymes break down glycerides, proteins, and carbohydrates, enabling their absorption. On the other hand, the endocrine functions are related to the production of crucial hormones for the body, particularly insulin, which regulates blood glucose levels and is directly linked to diabetes (Zhou and Melton, 2018).

Pancreatic problems can lead to various health conditions, including pancreatitis (inflammation of the pancreas), diabetes (due to issues with insulin production), and pancreatic cancer. Among cancer types, pancreatic cancer, although relatively rare, is one of the deadliest. The survival rate for pancreatic cancer is one of the lowest among all tumor types, with a mortality rate of 98% (Chakrabarti et al., 2023), reflecting the severity and the challenge of early diagnosis due to the organ's location and characteristics in imaging exams. The most common type of pancreatic cancer is Pancreatic ductal adenocarcinoma (PDAC), accounting for 90% of diagnosed cases (Stoffel et al., 2023). PDAC typically affects the right side of the organ (the head). The other parts of the pancreas are the body (central region) and the tail (left side), and they can be observed in the Figure 1.

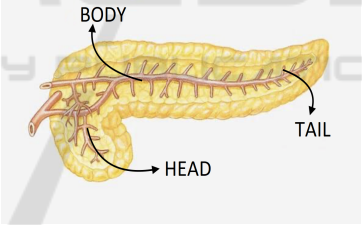

Figure 1: Pancreas anatomy.

The factors driving the lethality of PDAC are numerous, centered on an inability to detect the disease until late in progression, often after distant metastasis (Kleeff et al., 2016). Moreover, outside of the minority (10%–15%) of cases ascribed to germline mutations or known risk factors, such as mucinous cystic lesions and chronic pancreatitis, there is no sin-

[a] https://orcid.org/0000-0002-0250-6211
[b] https://orcid.org/0000-0001-7013-9700
[c] https://orcid.org/0000-0003-4921-0626

Faray de Paiva, F., Araujo, A. C., Sousa de Almeida, J. D. and C. de Paiva, A.
Pancreatic Mass Segmentation Using TransUNet Network.
DOI: 10.5220/0013292200003929

In *Proceedings of the 27th International Conference on Enterprise Information Systems (ICEIS 2025) - Volume 1*, pages 512-522
ISBN: 978-989-758-749-8; ISSN: 2184-4992

gle attributable risk factor for most patients (Petersen, 2016).

According to the Union for International Cancer Control (UICC), cases of pancreatic cancer increase with age: from 10 per 100,000 inhabitants between 40 and 50 years old to 116 per 100,000 inhabitants between 80 and 85 years old, with a more significant incidence in males (Choe et al., 2019). Diagnosing this type of cancer is challenging, as cancerous tumors exhibit low texture divergence from normal pancreatic tissue.

Pancreatic cancer is a significant global health concern, with rising incidence and mortality rates observed over recent years. In 2020, approximately 495,773 new cases were diagnosed worldwide, leading to 466,003 deaths, making it the 7th leading cause of cancer-related mortality (Seufferlein and Kestler, 2023) (Moradi et al., 2022). Identifying early diagnosis options is an important way to improve detection and survival rates of pancreatic cancer. None of the many tumor markers associated with pancreatic cancer are highly specific, which also indicates further research is required to improve the early detection rate (Zhao and Liu, 2020). In Computer-Aided Diagnosis (CAD) for pancreatic cancer diagnosis, the first step is commonly the automatic segmentation of the organ (Chu et al., 2017). The segmentation of the pancreas and masses within the organ presents different factors that complicate this process, such as low contrast among soft tissue within the organ, low contrast between the pancreas and adjacent organs (liver, spleen, and stomach), and high anatomical variation, meaning that the location in the abdominal cavity and the shape of the pancreas vary significantly from patient to patient (Liu et al., 2019). Machine learning technologies such as CNNs and Natural Language Processing (NLP) are a powerful tool in CAD systems as they automatically learn features that define the target object to be segmented.

Transformers are now the state-of-the-art in many NLP tasks (Vaswani, 2017), it's success in NLP has inspired several methods in computer vision, combining CNNs with forms of self-attention to address semantic segmentation (Fan et al., 2024). In this context, this work aims to explore using Transformer networks to segment masses in the pancreas.

Early diagnosis is crucial in treatment, potentially increasing patient survival rates up to 50% (Conroy et al., 2018). Therefore, aiming to support the early diagnosis, this work explores a CAD system utilizing a transformer-based network. The objective of this work is to propose a new computational method for segmenting masses in the pancreas using Transformer networks.

2 RELATED WORK

The segmentation of the pancreas and its masses in CT images plays a crucial role in supporting medical specialists in identifying pancreatic cancer. Various computational approaches are employed to improve diagnostic accuracy and reduce the risks associated with other imaging techniques, such as radiology or invasive procedures like biopsies. In recent years, the focus has been on developing and applying advanced image processing and deep learning techniques, aiming to refine the segmentation of both the pancreas and pancreatic tumors. This section provides a review of the most recent studies, conducted over the past five years, exploring these technological advancements in the context of pancreatic mass segmentation.

In recent years, segmentation using Transformer networks has gained prominence in the literature due to their ability to capture global interactions in medical images. Studies such as those by Wang et al. (Wang et al., 2022) have demonstrated that this combination improves semantic segmentation accuracy, making it more robust against typical challenges in medical images, such as low contrast and anatomical variations. The flexibility of Transformers in modeling complex long-term interactions, without relying solely on local relationships, allows for more detailed and precise segmentation, which is essential in applications like tumor identification in organs such as the pancreas. He et al. (He et al., 2023) highlighted that Transformers can effectively model complex anatomical variations and global interactions, overcoming the limitations of CNN-based approaches. Additionally, the work of Su et al. (Su et al., 2022) shows that using Transformers in CAD systems facilitates mass identification and segmentation, promoting earlier and more accurate diagnoses, which is crucial for increasing patient survival rates.

The most commonly used dataset is the Medical Segmentation Decathlon (MSD) (Antonelli et al., 2022), which includes annotations for the pancreas and masses. This dataset contains annotations for different organs and their internal structures; however, this section focuses solely on the performance of pancreatic mass segmentation. For the segmentation of pancreatic masses in CT images, 9 studies were found and selected.

The automatic adaptation of the model to the problem is an approach for this scope, where the model adjusts its architecture (Zhu et al., 2019)) or parameters (Isensee et al., 2018)) during training. In the work of Zhu et al. (Zhu et al., 2019), a method for automatic architecture search for segmentation networks

is proposed. Specifically, at each layer, the network selects which type of convolutions to use (2D, 3D, or pseudo-3D) to construct an encoder-decoder network. Meanwhile, Isensee et al.(Isensee et al., 2018) proposed the nn-Unet network, a self-configuring method based on 3D-Unet that adapts to the dataset using three types of parameters: fixed, rule-based, and empirical. The self-configuring nature of this method allows it to perform well in various biomedical applications. These studies achieved average DSCs of 37.78±32.12% and 52.27% in pancreatic mass segmentation, respectively. Yang et al. (Yang et al., 2021) propose a neural network based on Local Linear Embedding (LLE) for interpolation. The embedding models the relationships between adjacent and interpolated slices, while the neural network, combined with the LLE module, enhances image resolution to generate better images for each sequence. The proposed network achieved an average Dice score of 50.6% with a standard deviation of 30.9%.

Mahmoudi et al. (Mahmoudi et al., 2022) proposed cascade segmentation methods for the mass. They initially perform pancreas localization using a 3D Fully Connected Network (FCN) with a 3D Local Binary Pattern. After the localization step, once the areas of interest are identified, the mass segmentation is conducted using the Textured U-Net, a proposed architecture.

Cao and Li (Cao and Li, 2024) also utilizes a cascade approach. Initially, an Attention U-Net is used to localize the pancreas. Next, the segmentation of both the pancreas and the mass is carried out. The input image is sent to the Decoder along with a spatial information retrieval mechanism that replaces the Skip Connections, providing the Decoder with hierarchically extracted information from the Encoder, combined with information that may have been lost during processing but is present in the original image. Additionally, features are extracted in parallel through three convolution paths with different dilatations, merged at the end with the output of the Encoder-Decoder to produce the final segmentation based on features at different resolutions. The authors apply the network separately for pancreas and mass segmentation, achieving a Dice score of 54.38 ± 1.70% for the mass. Although the mean is not as high as in other works, the low standard deviation demonstrates the model's stability.

Another approach targets the pancreas and mass simultaneously. Using three modules—Temperature Balance Loss, Rigid Temperature Optimizer, and Temperature Indicator—the model balances the weight between the pancreas and mass classes so that mass learning is improved without significant loss in pancreas learning. The result obtained on the MSD dataset was 59.16% ± 28.12% Dice for mass segmentation in the pancreas.

Table 1 summarizes the selected studies in the literature for pancreatic mass segmentation. Among these, it is noteworthy that a high standard deviation is present in almost all studies, except for Cao and Li, (Cao and Li, 2024), which, despite having a lower mean Dice performance, demonstrates superior performance regarding standard deviation.

Given the studies explored in this chapter, the proposed method aims to investigate the efficiency of Transformer mechanisms combined with CNNs through the TransUNet network (Chen et al., 2021) and its application to CT images. The image dataset from the Medical Segmentation Decathlon (MSD) was used for evaluation and comparison with the cited studies concerning pancreatic mass segmentation.

3 TransUNet NETWORK

The TransUNet network, proposed by Chen et al. (Chen et al., 2021), is a hybrid architecture that combines the global dependency-capturing capability of Transformers with the spatial detail-preserving ability of U-Net. The model uses a Transformer as an encoder to capture large-scale contextual relationships, followed by a U-Net-based decoder to recover fine details and perform precise segmentation of medical images, as illustrated in Figure 2.

The structure begins with a Transformer-based encoder, where the input image is divided into small patches (typically 16x16 pixels), a technique inspired by the Vision Transformer (ViT) proposed by (Dosovitskiy, 2020). Each patch is "flattened" into a sequence of numbers and then transformed into a vector with more relevant features through a linear layer, a process known as embedding, which creates a dense and continuous representation of the patches, allowing the model to work with them more efficiently.

Since Transformers, originally introduced by (Vaswani, 2017), lack an intrinsic structure to capture the position of elements, a positional encoding vector is added to each embedding to preserve the spatial order of the patches, enabling the model to understand the relative location of different patches in the original image. The embedding sequence is illustrated in Figure 2, above the ViT layer.

After the encoding step done by the Transformers, TransUNet uses a U-Net-style decoder (Ronneberger et al., 2015), which reconstructs the original image resolution through upsampling and convolutions. This process is supported by skip connections

Table 1: Comparison of segmentation methods with their respective performances and standard deviations.

Authors	Method	DSC by patient (%)
(Ju et al., 2023)	Spacial Visual Cues Fusion (SVCF) Active Localization OffseT (ALOT)	63.36
(Mahmoudi et al., 2022)	Texture Attention U-Net (TAU-Net)	60.6
(Li et al., 2023)	Temperature Guided 3D FCN	59.16 ± 28.12
(Cao and Li, 2024)	Strongly Representative Semantic-guided Segmentation Network (SRSNet)	54.38 ± 1.7
(Turečková et al., 2020)	V-Net	52.99
(Isensee et al., 2018)	nn-Unet	52.27
(Yang et al., 2021)	Local Linear Embedding Interpolation Neural Network	50.6 ± 30.9
(Li et al., 2020)	Position Guided Deformable U-Net (PDF-Unet)	50.12 ± 30,86
(Zhu et al., 2019)	V-Nas	37.78 ± 32.12

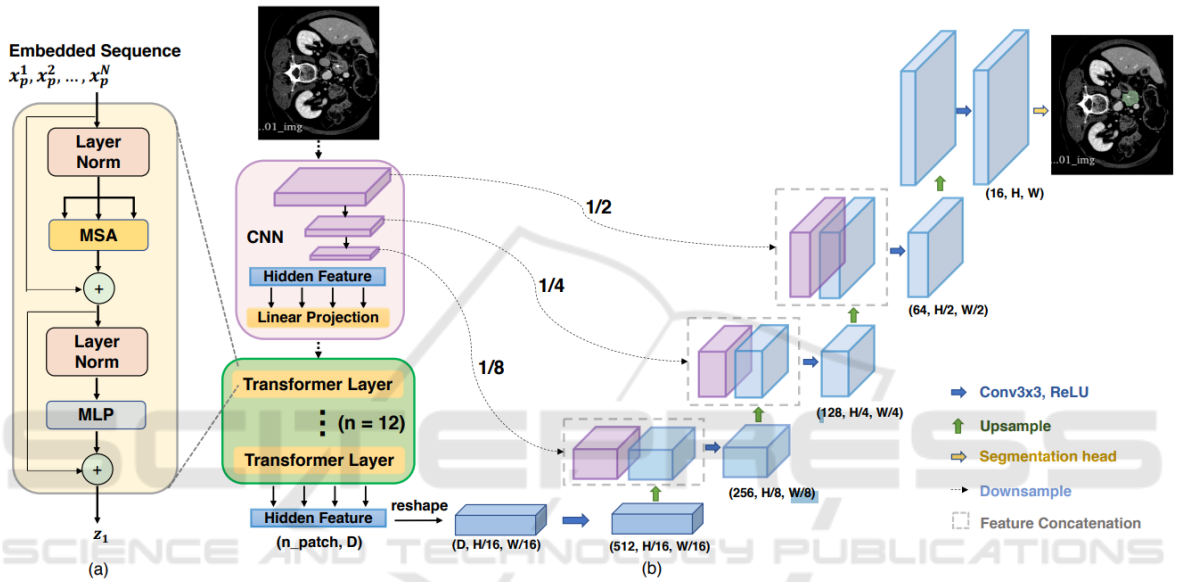

Figure 2: TransUNet's architecture (Chen et al., 2021).

between corresponding encoder and decoder layers, allowing spatial details captured during encoding to be directly used in decoding. These connections are crucial to ensure that the final segmentation is accurate, combining global information extracted by the ViT layers with local details provided by U-Net.

This combination makes TransUNet effective in capturing global contexts and local details, essential for complex segmentations in medical images, where edge precision and global anatomical context are necessary (Chen et al., 2021).

Instead of using a pure Transformer as the encoder, TransUNet employs a hybrid CNN-Transformer model, where the CNN is initially used as a feature extractor to generate a feature map from the input. Subsequently, patch embedding is applied to 1x1 patches extracted from the CNN's feature map instead of directly from raw images. This allows for leveraging the high-resolution intermediate feature maps of the CNN in the decoding path and demonstrates superior performance compared to using a pure Transformer as the encoder.

A Cascaded Upsampling Path (CUP) is used in the network and consists of multiple upsampling steps to decode hidden features and generate the final segmentation mask. After reshaping the hidden feature sequence $z_L \in \mathbb{R}^{\frac{HW}{P^2} \times D}$ to the form $\frac{H}{P} \times \frac{W}{P} \times D$, the CUP is instantiated by chaining multiple upsampling blocks to achieve the full resolution of $\frac{H}{P} \times \frac{W}{P}$ to $H \times W$, where each block consists of a 2× upsampling operators, a 3×3 convolutional layer, and a ReLU layer, which eliminates negative numbers by comparing them with 0 and selecting the higher value.

The CUP and the hybrid encoder form a "U"-shaped architecture, enabling the aggregation of features at different resolution levels through skip connections. The detailed architecture of the CUP and the intermediate skip connections can be found in Figure 2.

4 MATERIALS AND METHOD

This section outlines the materials used and the procedures employed to conduct the study. It details the dataset, preparation techniques, analytical methods, and statistical tools used to ensure reliable results. By describing each step, this section provides a clear understanding of the experimental setup and methodology.

Figure 3 outlines the method implemented in this work step by step, starting by the raw data provided by the MSD dataset, a volume of the CT from a patient with dimensions 512 x 512 x z. Then we take in consideration only the slices with the presence of masses and apply on them a Hounsfield windowing to highlight the pancreas area. Before doing the k-fold division, for the experiment 2, we do a crop of a square near the pancreas area, with a size of 256 x 256. Now we perform the k-fold division by patient, taking in consideration that slices from the same patient could compromise the reliability of the results. After a simple Data augmentation the the data is provided to the network.

4.1 Dataset

In the experiments, the public dataset Medical Segmentation Decathlon (MSD) was selected, specifically Challenge 7 for pancreatic mass segmentation (Antonelli et al., 2022), which includes CT images from the venous phase of the full torso. The Memorial Sloan Kettering Cancer Center in New York provides the scans. The reconstruction and acquisition settings were: automatic tube current modulation range, 220–380 mA; pitch/table speed, 0.984–1.375/39.37–27.50 millimeters; noise index, 12.5–14; 120 kVp; tube rotation speed, 0.7–0.8 ms; scan delay, 80–85 s; and axial slices reconstructed at 2.5 mm intervals.

The dataset contains three types of masses: Pancreatic Adenocarcinoma, Pancreatic Neuro-endocrine Tumor, and Intraductal papillary mucinous neoplasms. However, it does not provide any indicative labeling to differentiate among them within the dataset. A specialist manually marked the segmentation of the pancreatic parenchyma and the mass (cyst or tumor) in the dataset using the scout application.

A total of 420 CT scans are available, but only 281 include radiologist annotations for training, while the remaining 139 are reserved exclusively for challenge testing. All experiments in this research were conducted solely on the training set (with annotations), following the standard in the literature; for example, Cao and Li (Cao and Li, 2024), Li et al. (Li et al., 2023) and Ju et al.(Ju et al., 2023).

Figure 4 shows how the raw data is provided by the dataset, which originally consisted of files in the NIFTI format, characterized by volumes with a resolution of 512x512 and variable height depending on the patient, with a minimum value of 37 and a maximum of 751.

4.2 Pre-Processing

This step standardizes the input data and improves the network's effectiveness by increasing the contrast of the object of interest relative to non-relevant tissues. The Hounsfield Unit (HU) windowing technique is widely used in computed tomography (CT) to optimize the visualization of different tissue types in medical images. HU values are a quantitative scale reflecting tissue density compared to water, which has a value of 0 HU. Air, for instance, has a value of -1000 HU, while bone tissues can reach values above 1000 HU. The windowing technique allows for adjusting the range of Hounsfield values displayed in the image, explicitly highlighting the tissues of interest. This adjustment is performed by setting the upper and lower thresholds, which are defined according to Equations (1) and (2), respectively:

$$\text{upper threshold} = \text{center} + \frac{\text{width}}{2} \quad (1)$$

$$\text{lower threshold} = \text{center} - \frac{\text{width}}{2} \quad (2)$$

Any HU value greater than the upper threshold is truncated to the upper threshold value, and any HU value lower than the lower threshold is truncated to the lower threshold value.

Hounsfield windowing was performed for all reserved slices with masses. The center and width values used, according to Equations 2 and 1, were 50 and 400, respectively. This adjustment changed the original CT window, ranging from -4096 to 2048 HUs, to a range of -150 to 250 HUs. According to Mo et al.(Mo et al., 2020), this interval enhances soft tissues in the abdomen, a category to which the pancreas belongs. In the pre-processing phase, the data, initially provided in NIFTI format containing the patient's complete CT volume, were limited to slices with masses. After this step, the data were split into four folds, each containing 25% of the total number of patients, and basic data augmentation techniques, such as orthogonal rotation and random inversion along the x and y axes, were applied.

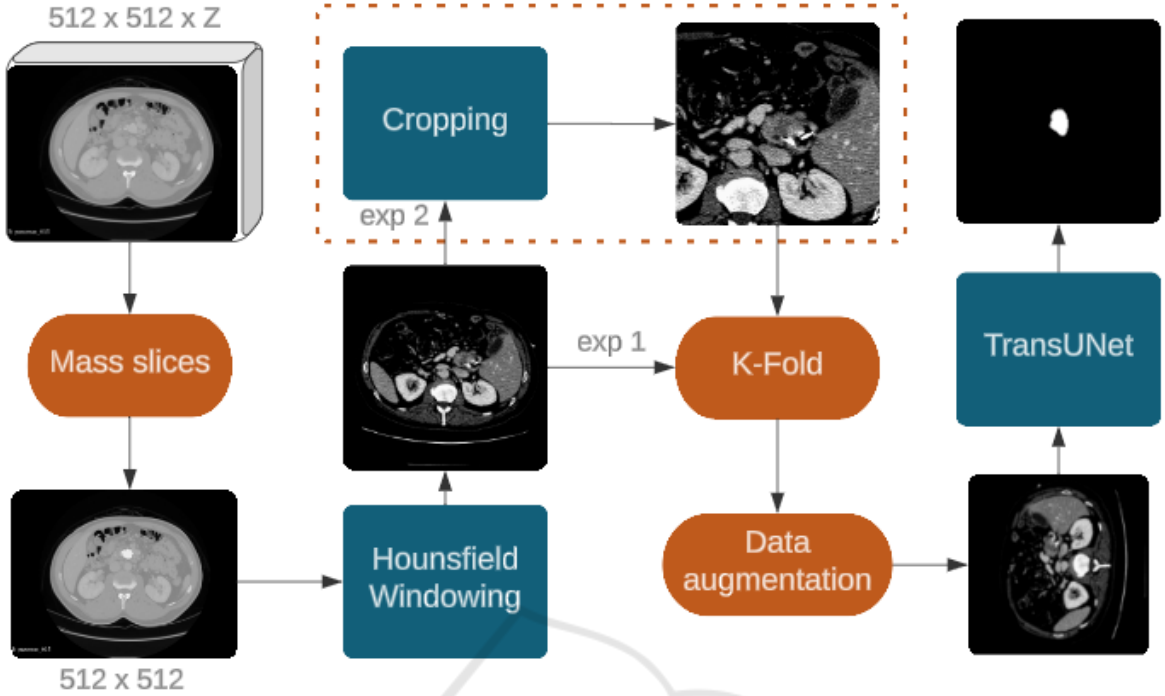

Figure 3: Method proposed.

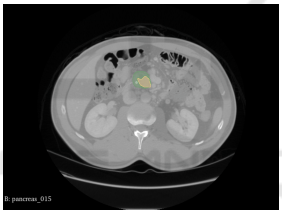

(a) axial slice

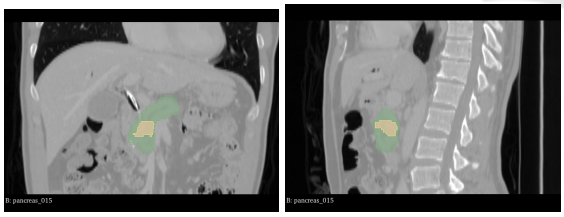

(b) coronal slice (c) sagittal slice

Figure 4: Examples from MSD base. Green notattion for pancreas and yellow for masses.

4.3 Cropped Slice

This work highlights two experiments conducted. One is more general and closer to real-world scenarios, applying some pre-processing steps to the data and providing them to the network, as shown in Figure 2. The other experiment focuses more specifically on segmenting the pancreatic mass, as a cropping technique is applied around the mass region before performing the segmentation. The configurations and results of both experiments will be presented below.

4.3.1 Experiment 1:Full Slice

In the first experiment, the complete slices were used as input. The input resolution and patch size are 512x512 and 16, respectively. Each fold was trained for 200 epochs with a batch size of 4. Figure 5 provides examples of how the images were fed into the network.

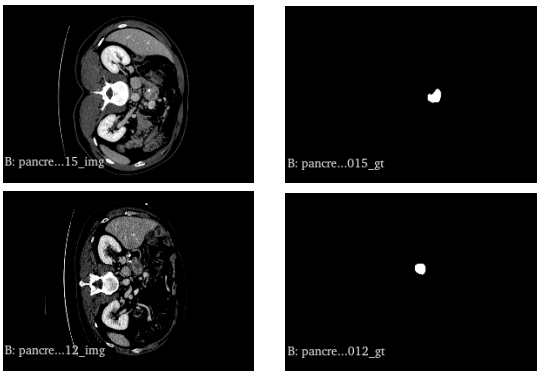

Figure 5: Examples of full slices on the left side and their respective masks on the right side.

4.3.2 Experiment 2: Cropped Slice

In the second experiment, a crop of the complete slices of the patients were performed and used as input. The resolution and patch size used were 256x256 and 16, respectively. Each fold was trained for 200 epochs with a batch size of 16. Figure 6 provides examples of how the images were fed into the network. This crop was performed by locating the central point of the mass in the mask and then extracting a 256x256 square. By cropping the region of interest, the model focuses on the parts of the image containing relevant information for the specific task, which, in this case, is mass segmentation. This reduces the amount of irrelevant or background information the model needs to process, increasing accuracy by highlighting only the data directly important for prediction. Since the mass comprises a tiny region of the image, the cropping technique can be highly effective. Increasing the batch size from 4 to 16 improves gradient stability and smoothness, meaning weight updates during training become more consistent, helping the model converge more quickly. Additionally, larger batches are more efficient for parallel processing on GPUs, which speeds up training time per iteration. Figure 6 presents examples of the input data used for the network in this experiment.

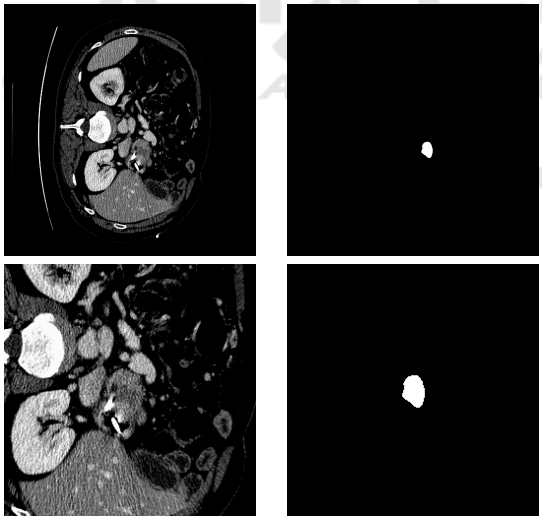

(A) (B)

Figure 6: In A original and crop, in B their respective masks.

A significant increase in the proportion of the mass size relative to the image size can be observed, enhancing the prominence of the segmentation target and consequently facilitating the network's training.

4.4 TransUnet Training

For the network's hybrid encoder, a combination of ResNet-50 (He et al., 2016) and ViT (Vaswani, 2017), termed "R50-ViT", as presented by Chen et al.(Chen et al., 2021), was chosen. All Transformers (i.e., ViT) and ResNet-50 backbones (referred to as "R-50") were pre-trained on ImageNet (Deng et al., 2009).

All 3D volumes were trained and inferred slice-by-slice, and the predicted 2D slices were stacked to reconstruct the 3D prediction for evaluation. In the network's training phase, the average between Cross-Entropy Loss and Dice Loss was used as the loss function. Each is described by Equations 3 and 4, respectively. Since Cross-Entropy Loss effectively captures the correct probability for each pixel or voxel, while Dice Loss focuses on the overlap of the segmented classes, this selection aimed to improve local accuracy and overall segmentation.

$$L_{CE} = -\sum_{i=1}^{N} T_i \log(P_i) \tag{3}$$

$$L_{Dice} = 1 - \frac{2\sum_{i=1}^{N} P_i T_i + \varepsilon}{\sum_{i=1}^{N} P_i + \sum_{i=1}^{N} T_i + \varepsilon} \tag{4}$$

Where "T" represents the target set, the ground truth masks the images as defined by experts, and "P" is the set of predictions generated by the network.

The models were trained using the SGD optimizer with a learning rate set to 0.0001, momentum of 0.9, and weight decay of 1e-4.

4.5 Experiments

All experiments were conducted on hardware configured with an NVIDIA GeForce GTX 3060 GPU with 12 GB of VRAM.

The cross-validation technique was used for model evaluation, which involves splitting the dataset into folds for training and testing, as mentioned previously. In this research, a 4-fold division was chosen. A different test is performed for each fold, with the remaining folds used for training in each test. This increases evaluation confidence and tests the influence of data variation on the network, thereby determining the model's generalization.

4.6 Evaluation Metrics

The evaluation metrics used were the Dice coefficient (D), described in Equation 5, and the HD95 metric (Hausdorff Distance at 95th percentile), described in Equation6. The Dice coefficient aims to measure the

similarity between two samples, which, in the context of this work, represents the similarity between the generated predictions and the reference values (Taha and Hanbury, 2015).

$$DSC = \frac{2 \times TP}{2 \times TP + FP + FN} \quad (5)$$

Where "TP" means True Positives, which represents pixels correctly classified as mass; "FP" means False Positives, which consists of pixels incorrectly classified as mass; and "FN" is False Negatives that represents pixels incorrectly classified as not being mass. The HD95 metric (Hausdorff Distance at 95th percentile) is a variation of the Hausdorff Distance (HD), which measures the maximum discrepancy between two sets of points (such as contours in segmented images) (Taha and Hanbury, 2015). While the traditional Hausdorff Distance considers the maximum value of all distances, HD95 only considers the 95th percentile of the distances, making it less sensitive to outliers and more robust for evaluating the similarity between two segmentations.

$$\text{HD95}(P,T) = \max \left\{ \sup_{p \in P} \inf_{t \in T} \|p - t\|, \sup_{t \in T} \inf_{p \in P} \|t - p\| \right\} \quad (6)$$

'inf' represents the shortest distance between a point x from a set X and Y, 'sup' selects the largest minimum distance (inf), and 'max' takes the highest value between the two suprema.

5 RESULTS AND DISCUSSION

This section highlights and discuss the results from the previously commented experiments.

5.1 Results from Full Slices

The experiment 4.3.1, which refers to a more general and complex segmentation, mainly due to the lack of detail, achieved an average DICE of approximately 0.426 and an average HD of 17.58. The complete cross-validation results are shown in Table 2.

Table 2: Pancreatic mass segmentation for Full slices of the patients.

Folds	↑ Dice (%)	↓ HD95
Fold 1	41.37	14
Fold 2	42.98	20
Fold 3	40.42	21
Fold 4	45.61	15.3
Average	**42.60±1.97**	**17.58**

Analyzing the average HD value, it can be observed that the shape of the mass segmented by the model approximated the expert's annotation; however, there is still room for improvement. Examples of the predictions can be found in Figure 7.

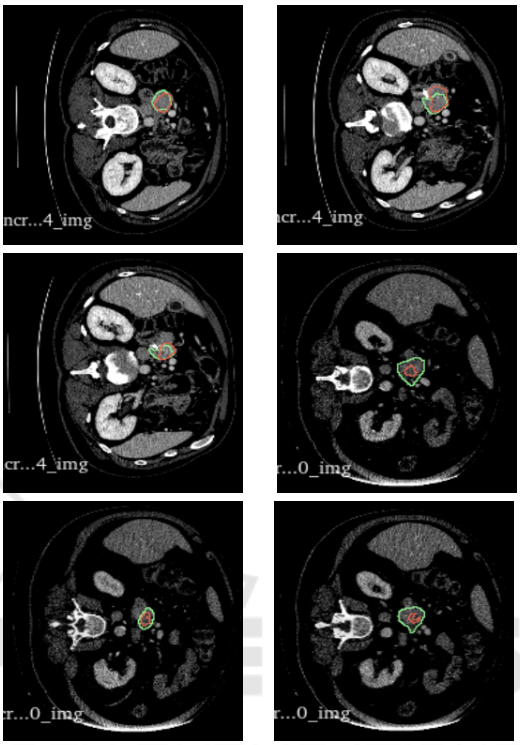

Figure 7: Examples of predictions from the TransUNet network in fold number 4. The red marking indicates the network's prediction, while the green marking represents the expert's annotation.

5.2 Results from Cropped Segmentation

The results of the cross-validation for experiment from cropped region segmentation are presented in the Table 3.

Table 3: Pancreatic mass segmentation for the cropped slices.

Folds	↑ Dice (%)	↓ HD95
Fold 1	81.41	4.12
Fold 2	79.92	4.12
Fold 3	75.82	7.87
Fold 4	81.51	6.63
average	**79.67±2.31**	**5.69**

It showed a very promising Dice score average of 79.67%, with a good standard deviation of 2.31, these results are 16.31% up in comparing with the State of the Art (Ju et al., 2023).Analyzing the HD95, we can observe that the network produced a segmenta-

tion very close to the expert's annotation. For example, Figure 8 shows segmentation examples in good, medium and relatively poor cases in decreasing order.

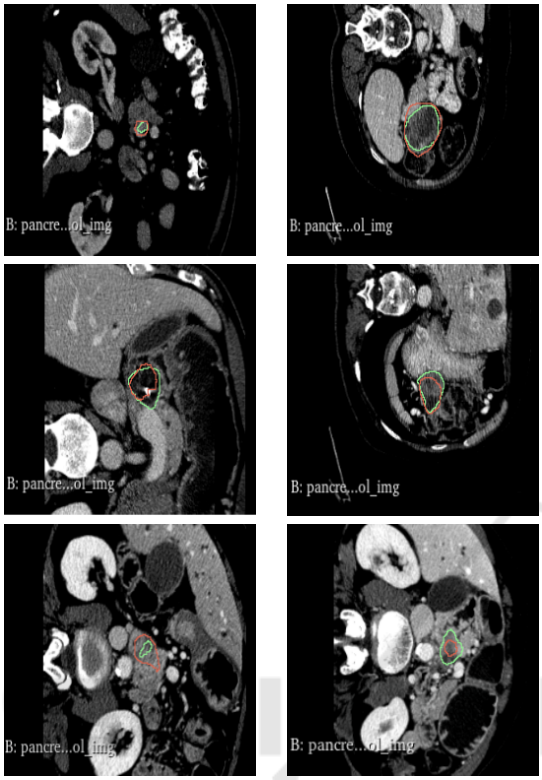

Figure 8: Examples of TransUNet network predictions in fold 4 for the cropped region. The red marking indicates the network's prediction, while the green marking represents the expert's annotation.

In comparing the method with the literature, this work uses the nine other studies described in section 2. Table 4 presents the studies in descending order of Dice score.

As observed from the standard deviation in each case (among those providing this information), all results tend to be highly volatile. At the same time, the method used here shows low variation, specifically the second-lowest reported in the literature.

Thus, it can be concluded that, after an initial localization of the target object, the TransUNet network performs excellently for pancreatic mass segmentation, achieving an average Dice score of 79.67 with a standard deviation of 2.31%. However, it is worth noting that extracting the crop based on the mass center may influence the results, as the target object is always centered.

It was also noted that the network is more effective in segmenting masses with a more rounded shape and less effective for irregularly shaped masses. These results indicate that, in a scenario with precise localization of the mass region, the method is significantly more effective than the state-of-the-art (Ju et al., 2023) for pancreatic mass segmentation. However, its performance in more general segmentation, covering the entire CT data, is less satisfactory, with an average Dice score of 42.60%, despite being quite consistent, as indicated by a standard deviation of ±1.97

6 CONCLUSION

Early diagnosis is a crucial factor in disease outcomes, as patients diagnosed at stage 1 can have a more favorable prognosis, with up to 80% survival over five years. This study aimed to propose methods that reduce the number of late diagnoses (Cheng, 2018).

One of the main challenges for early diagnosis of pancreatic cancer is the pancreas's small size, its low contrast compared to adjacent structures, and pancreatic tissue in imaging exams, such as computed tomography. Additionally, computed tomography generates several images, making manual analysis challenging. In this context, computational methods play an essential role, as they can assist in diagnosis by reducing analysis time and helping identify pathologies.

In this work, two methods were proposed. The first method involved applying the TransUNet network for images from the MSD Dataset. This method was designed for pancreatic masses segmentation from the complete CT slice. While its results showed limitations, it also presented a low standard deviation. The second method required the initial detection of the mass region, and then, from this ROI, the pancreatic mass segmentation was performed, enhancing the target's prominence. This method presents the limitation of the requirement of a previous ROI detection phase but presents better results for the segmentation.

This work indicated the potential of deep learning techniques, such as the TransUNet network, for segmenting pancreatic mass from CT scans. Even with the challenges posed by the pancreas's small size and low contrast, these techniques show promise in improving the early diagnosis of pancreatic cancer. The experiments also highlight insights into the importance of focusing the segmentation on the region of interest that contains the mass to improve the segmentation method performance, as shown in the second proposed method. The work also underscores the urgent need for further research to explore the automatic detection of the mass ROI and the exploration of data augmentation techniques to increase the robustness of

Table 4: Comparison of segmentation methods with their respective performances and standard deviations.

Authors	Method	DSC by patient (%)
This work	**TransUNet with crop**	**79.67±2.31**
(Ju et al., 2023)	Spacial Visual Cues Fusion (SVCF) Active Localization OffseT (ALOT)	63.36
(Mahmoudi et al., 2022)	Texture Attention U-Net (TAU-Net)	60.6
(Li et al., 2023)	Temperature Guided 3D FCN	59.16 ± 28.12
(Cao and Li, 2024)	Strongly Representative Semantic-guided Segmentation Network (SRSNet)	54.38 ± 1.7
(Turečková et al., 2020)	V-Net	52.99
(Isensee et al., 2018)	nn-Unet	52.27
(Yang et al., 2021)	Local Linear Embedding Interpolation Neural Network	50.6 ± 30.9
(Li et al., 2020)	Position Guided Deformable U-Net (PDF-Unet)	50.12 ± 30.86
This work	**TransUNet**	**42.4 ± 2.6**
(Zhu et al., 2019)	V-Nas	37.78 ± 32.12

the models. This emphasis on the need for continuous research highlights this work's importance and potential impact.

The relevance of the proposed work lies in its contribution to the development of computational tools that can assist in the early diagnosis of pancreatic cancer, a disease with a poor prognosis when detected late. The work propositions have the potential to help healthcare professionals identify pancreatic masses earlier and, after improvements and validation, contribute to better treatment outcomes for patients.

Validation of the second proposed method by introducing positional shifts to the mass would be a valuable direction. Additionally, developing a detection, a kind of gross segmentation followed by a more detailed segmentation step, appears promising, as the initial results of this experiment were positive. Further investigation into advanced pre-processing methods to enhance the visibility of the pancreatic mass, such as wavelet or Fourier transforms, could also yield significant improvements. These proposed steps are intended to improve the practical applicability of the methods, bringing them closer to potential clinical deployment.

ACKNOWLEDGMENTS

The authors acknowledge the Coordenação de Aperfeiçoamento de Pessoal de Nível Superior (CAPES), Brazil - Finance Code 001, Conselho Nacional de Desenvolvimento Científico e Tecnológico (CNPq), Brazil, and Fundação de Amparo à Pesquisa Desenvolvimento Científico e Tecnológico do Maranhão (FAPEMA) (Brazil), Empresa Brasileira de Serviços Hospitalares (Ebserh) Brazil (Grant number 409593/2021-4) for the financial support.

REFERENCES

Antonelli, M., Reinke, A., Bakas, S., Farahani, K., Kopp-Schneider, A., Landman, B. A., Litjens, G., Menze, B., Ronneberger, O., Summers, R. M., et al. (2022). The medical segmentation decathlon. *Nature communications*, 13(1):4128.

Cao, L. and Li, J. (2024). Strongly representative semantic-guided segmentation network for pancreatic and pancreatic tumors. *Biomedical Signal Processing and Control*.

Chakrabarti, G. et al. (2023). Diagnosing and monitoring pancreatic cancer through cell-free dna methylation: progress and prospects. *Biomarker Research*, 11:12–34.

Chen, J., Lu, Y., Yu, Q., Luo, X., Adeli, E., Wang, Y., Lu, L., Yuille, A. L., and Zhou, Y. (2021). Transunet: Transformers make strong encoders for medical image segmentation. *arXiv preprint arXiv:2102.04306*.

Cheng, S. (2018). *Punção ecoendoscópica de massas sólidas pancreáticas por técnica de pressão negativa versus capilaridade: estudo prospectivo e randomizado*. PhD thesis, Universidade de São Paulo, São Paulo, Brasil.

Choe, J., Kim, K. W., Kim, H. J., Kim, D. W., Kim, K. P., Hong, S.-M., Ryu, J.-S., Tirumani, S. H., Krajewski, K., and Ramaiya, N. (2019). What is new in the 2017 world health organization classification and 8th american joint committee on cancer staging system for pancreatic neuroendocrine neoplasms? *Korean journal of radiology*, 20(1):5–17.

Chu, L. C., Goggins, M. G., and Fishman, E. K. (2017). Diagnosis and detection of pancreatic cancer. *The Cancer Journal*, 23(6):333–342.

Conroy, T., Hammel, P., Hebbar, M., Ben Abdelghani, M., Wei, A. C., Raoul, J.-L., Choné, L., Francois, E., Artru, P., Biagi, J. J., et al. (2018). Folfirinox or gemcitabine as adjuvant therapy for pancreatic cancer. *New England Journal of Medicine*, 379(25):2395–2406.

Czako, L., Hegyi, P., Rakonczay, Z., Wittmann, T., and Otsuki, M. (2009). Interactions between the endocrine and exocrine pancreas and their clinical relevance. *Pancreatology*, 9(4):351–359.

Deng, J., Dong, W., Socher, R., Li, L.-J., Li, K., and Fei-Fei, L. (2009). Imagenet: A large-scale hierarchical image database. In *2009 IEEE conference on computer vision and pattern recognition*, pages 248–255. Ieee.

Dosovitskiy, A. (2020). An image is worth 16x16 words: Transformers for image recognition at scale. *arXiv preprint arXiv:2010.11929*.

Fan, X., Zhou, J., Jiang, X., Xin, M., and Hou, L. (2024). Csap-unet: Convolution and self-attention paralleling network for medical image segmentation with edge enhancement. *Computers in Biology and Medicine*, 172:108265.

He, K., Gan, C., Li, Z., Rekik, I., Yin, Z., Ji, W., Gao, Y., Wang, Q., Zhang, J., and Shen, D. (2023). Transformers in medical image analysis. *Intelligent Medicine*, 3(1):59–78.

He, K., Zhang, X., Ren, S., and Sun, J. (2016). Deep residual learning for image recognition. In *Proceedings of the IEEE conference on computer vision and pattern recognition*, pages 770–778.

Isensee, F., Petersen, J., Klein, A., Zimmerer, D., Jaeger, P. F., Kohl, S., Wasserthal, J., Koehler, G., Norajitra, T., Wirkert, S., et al. (2018). nnu-net: Self-adapting framework for u-net-based medical image segmentation. *arXiv preprint arXiv:1809.10486*.

Ju, J., Li, J., Chang, Z., Liang, Y., Guan, Z., Xu, P., and Xie, F. (2023). Incorporating multi-stage spatial visual cues and active localization offset for pancreas segmentation. *Pattern Recognition Letters*.

Kleeff, J., Korc, M., Apte, M., La Vecchia, C., Johnson, C. D., Biankin, A. V., Neale, R. E., Tempero, M., Tuveson, D. A., Hruban, R. H., et al. (2016). Pancreatic cancer. *Nature reviews Disease primers*, 2(1):1–22.

Li, Q., Liu, X., He, Y., Li, D., and Xue, J. (2023). Temperature guided network for 3d joint segmentation of the pancreas and tumors. *Neural Networks*.

Li, Z., Pan, H., Zhu, Y., and Qin, A. (2020). Pgd-unet: A position-guided deformable network for simultaneous segmentation of organs and tumors. In *2020 International Joint Conference on Neural Networks (IJCNN)*. IEEE.

Liu, S., Yuan, X., Hu, R., Liang, S., Feng, S., Ai, Y., and Zhang, Y. (2019). Automatic pancreas segmentation via coarse location and ensemble learning. *IEEE Access*, 8:2906–2914.

Mahmoudi, T., Kouzahkanan, Z., and Radmard, A. (2022). Segmentation of pancreatic ductal adenocarcinoma (pdac) and surrounding vessels in ct images using deep convolutional neural networks and texture descriptors. *Scientific Reports*.

Mo, J., Zhang, L., Wang, Y., and Huang, H. (2020). Iterative 3d feature enhancement network for pancreas segmentation from ct images. *Neural Computing and Applications*, 32:12535–12546.

Moradi, N., Doshantapeh, A. G., Sangi, S., Aligholizadeh, M., Asadian, A., Abdolmohammadi, G., Gharebakhshi, F., Abdolmohammadi, G., and Molaee, H. (2022). 4. an ecological study of the incidence and mortality rates of pancreatic cancer in 2020: exploring gender disparities worldwide. *Journal of renal endocrinology*.

Petersen, G. M. (2016). Familial pancreatic cancer. In *Seminars in oncology*, volume 43, pages 548–553. Elsevier.

Ronneberger, O., Fischer, P., and Brox, T. (2015). U-net: Convolutional networks for biomedical image segmentation. In *Medical image computing and computer-assisted intervention–MICCAI 2015: 18th international conference, Munich, Germany, October 5-9, 2015, proceedings, part III 18*, pages 234–241. Springer.

Seufferlein, T. and Kestler, A. M. R. (2023). 1. [exocrine pancreatic cancer - what is new in the update of the s3 guideline?]. *Deutsche Medizinische Wochenschrift*.

Stoffel, E. M., Brand, R. E., and Goggins, M. (2023). Pancreatic cancer: Changing epidemiology and new approaches to risk assessment, early detection, and prevention. *Gastroenterology*, 164(5):752–765. Personalizing GI Cancer Risk Assessment and Management: The Future is Now.

Su, Y., Liu, Q., Xie, W., and Hu, P. (2022). Yolo-logo: A transformer-based yolo segmentation model for breast mass detection and segmentation in digital mammograms. *Computer Methods and Programs in Biomedicine*, 221:106903.

Taha, A. A. and Hanbury, A. (2015). Metrics for evaluating 3d medical image segmentation: analysis, selection, and tool. *BMC Medical Imaging*, 15(1):29.

Turečková, A., Tureček, T., et al. (2020). Improving ct image tumor segmentation through deep supervision and attentional gates. *Frontiers in Robotics and AI*.

Vaswani, A. (2017). Attention is all you need. *arXiv preprint arXiv:1706.03762*.

Wang, T., Lan, J., Han, Z., Hu, Z., Huang, Y., Deng, Y., Zhang, H., Wang, J., Chen, M., Jiang, H., et al. (2022). O-net: a novel framework with deep fusion of cnn and transformer for simultaneous segmentation and classification. *Frontiers in neuroscience*, 16:876065.

Yang, X., Chen, Y., Yue, X., Ma, C., and Yang, P. (2021). Local linear embedding based interpolation neural network in pancreatic tumor segmentation. *Applied Intelligence*.

Zhao, Z. and Liu, W. (2020). Pancreatic cancer: a review of risk factors, diagnosis, and treatment. *Technology in cancer research & treatment*, 19:1533033820962117.

Zhou, Q. and Melton, D. A. (2018). Pancreas regeneration. *Nature*, 557(7705):351–358.

Zhu, Z., Liu, C., Yang, D., Yuille, A., et al. (2019). V-nas: Neural architecture search for volumetric medical image segmentation. In *2019 International Conference on Computer Vision (ICCV)*. IEEE.